



HAL
open science

Controlled release of gallium maltolate complex from injectable phosphocalcic cements

Manon Dupleichs, Maxence Limelette, Charlotte Mellier, Valérie Montouillout, François-Xavier Lefevre, Sophie Quillard, Jean-Yves Mevellec, Pascal Janvier

► **To cite this version:**

Manon Dupleichs, Maxence Limelette, Charlotte Mellier, Valérie Montouillout, François-Xavier Lefevre, et al.. Controlled release of gallium maltolate complex from injectable phosphocalcic cements. Materials Research Express, 2022, 9 (9), pp.095401. 10.1088/2053-1591/ac8a3c . hal-03791777

HAL Id: hal-03791777

<https://hal.science/hal-03791777>

Submitted on 29 Sep 2022

HAL is a multi-disciplinary open access archive for the deposit and dissemination of scientific research documents, whether they are published or not. The documents may come from teaching and research institutions in France or abroad, or from public or private research centers.

L'archive ouverte pluridisciplinaire **HAL**, est destinée au dépôt et à la diffusion de documents scientifiques de niveau recherche, publiés ou non, émanant des établissements d'enseignement et de recherche français ou étrangers, des laboratoires publics ou privés.

PAPER • OPEN ACCESS

Controlled release of gallium maltolate complex from injectable phosphocalcic cements

To cite this article: Manon Dupleichs *et al* 2022 *Mater. Res. Express* **9** 095401

View the [article online](#) for updates and enhancements.

You may also like

- [Determination of interlayer exchange fields acting on individual \(Ga,Mn\)As layers in \(Ga,Mn\)As/GaAs multilayers](#)
Sunjae Chung, Sangyeop Lee, Taehee Yoo et al.
- [Bias-dependent two-phase anisotropy in magnetoresistance of a GaMnAs-based magnetic tunnel junction](#)
Hiroshi Terada, Shinobu Ohya and Masaaki Tanaka
- [Coexistence of exchange bias and magnetization pinning in the MnO₂/GaMnAs system](#)
P W Huang, J H Huang, C H Yen et al.



The banner features the ECS logo on the left, a portrait of M. Stanley Whittingham with a Nobel Prize medal below it in the center, and a photograph of a lecture hall on the right. A 'Register now!' button with a checkmark icon is positioned above the lecture hall photo.

ECS The Electrochemical Society
Advancing solid state & electrochemical science & technology

242nd ECS Meeting
Oct 9 – 13, 2022 • Atlanta, GA, US
Presenting more than 2,400 technical abstracts in 50 symposia

ECS Plenary Lecture featuring M. Stanley Whittingham,
Binghamton University
Nobel Laureate – 2019 Nobel Prize in Chemistry

Register now!



PAPER

Controlled release of gallium maltolate complex from injectable phosphocalcic cements

OPEN ACCESS

RECEIVED
4 July 2022REVISED
3 August 2022ACCEPTED FOR PUBLICATION
16 August 2022PUBLISHED
6 September 2022

Original content from this work may be used under the terms of the [Creative Commons Attribution 4.0 licence](#).

Any further distribution of this work must maintain attribution to the author(s) and the title of the work, journal citation and DOI.

Manon Dupleichs¹, Maxence Limelette¹, Charlotte Mellier¹, Valérie Montouillout², François-Xavier Lefevre¹, Sophie Quillard³, Jean-Yves Mevellec³ and Pascal Janvier¹ ¹ Nantes Université, CNRS, CEISAM, UMR 6230, F-44000 Nantes, France² CEMHTI, CNRS UPR3079, Université Orléans, France³ Nantes Université, CNRS, Institut des Matériaux de Nantes Jean Rouxel, IMN, F-44000 Nantes, FranceE-mail: pascal.janvier@univ-nantes.fr**Keywords:** bone cancer, apatitic cement, drug delivery system, gallium maltolate, injectable cement, bone metastasesSupplementary material for this article is available [online](#)**Abstract**

Some cancers have tropism for bone: breast, prostate, lung, kidney, and thyroid cancers are the most common. Bone metastases can be treated with surgical resection and the resulting bone defects can be filled with injectable biomaterials. Among these, calcium phosphates may be the biomaterials of choice because of their ability to locally release anticancer active ingredients. Herein, we propose the synthesis of injectable calcium phosphate cement (CPC) loaded with gallium maltolate (GaM). It is an extremely promising anticancer drug with also antibiotic and anti-inflammatory properties. This synthesis was based on commercial cement whose main component was α -tri-calcium phosphate (α -TCP), and the final product obtained after hardening was calcium-deficient apatite (CDA). Two formulations were prepared, containing 3.5% and 7% by mass of GaM (CPC-3.5G and CPC-7G respectively). Powder x-ray diffraction (pXRD), Fourier transform infrared (FTIR) spectroscopy, and magic-angle spinning nuclear magnetic resonance (NMR MAS) ³¹P analyses showed that the direct incorporation of GaM did not modify the final cement composition. Textural properties, such as setting time, injectability, workability, and cohesiveness, were well preserved or even improved. Additionally, the mechanical strength, although slightly reduced, remained perfectly compatible with surgical use. *In vitro* kinetics studies of GaM-loaded CPCs showed a controlled release of GaM (49% at 60 days for CPC-3.5G and 58% at 116 days for CPC-7G) following Fick's law. Raman imaging was used to visualize its diffusion within the cement during *in vitro* release experiments. Finally, the structural integrity of the gallium complex in the CPC was confirmed using NMR MAS ⁷¹Ga.

1. Introduction

Bone tissue is a favorable environment for developing tumors (benign or malignant). Primary tumors are rare and primarily affect children, adolescents, and young adults. Alternatively, bone metastases have mainly been primarily observed in adults. This indicates the generalization of cancerous pathology, as in 65 to 75% of patients with breast or prostate cancer [1]. Despite advances in medical and surgical management, malignant bone tumors are associated with poor functional prognosis. Additionally, bone metastases can lead to complications such as fractures, hypercalcemia, or spinal cord compression [2]. In addition to systemic chemotherapy and/or radiation therapy, surgical resection of metastases and stabilization of pathological fractures are generally considered valuable palliative treatments [3]. Different materials have been used for bone reconstruction [4], among these, injectable calcium phosphate cements (CPCs) are particularly sought after because they not only adapt to the shape of a defect but also have primary mechanical properties analogous to those of trabecular bone. Even more, their ability to be used in minimally invasive surgery drastically extends their potential for use in clinical applications. However, this implies that separation occurred during injection [5]. Finally, they may act as

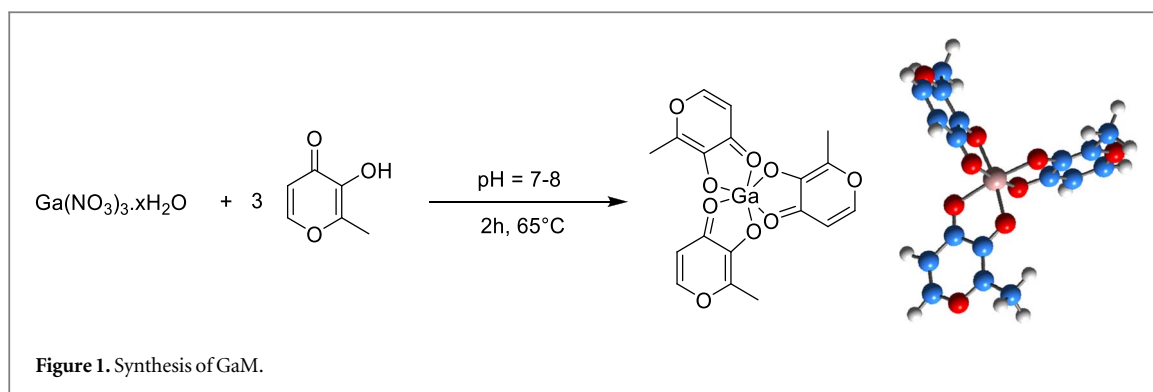
drug delivery systems for antibiotics, anti-inflammatory agents, or anticancer agents. Several studies have reported the addition of classical anticancer drugs to CPCs, to improve their effectiveness and tolerance [3, 6–10]. This local approach also reduces the risk of tumor resurgence in surrounding healthy tissues. Unfortunately, the toxicity of these drugs is inevitable and other alternatives such as gallium compounds must be developed. Because of its similarity to the Fe^{3+} ion, gallium can interfere with iron homeostasis. The use of ^{67}Ga has demonstrated the presence of this element in plasma, intimately bound to the iron transport protein, transferrin [11, 12]. This binding competition generates a decrease in the intracellular iron stocks in malignant cells and microorganisms with transferrin receptors. Consequently, iron-dependent cellular processes such as viability and growth are severely affected and may lead to cell apoptosis. Gallium nitrate has shown promising antineoplastic activity for the treatment of urothelial carcinoma, bladder carcinoma, and non-Hodgkin's lymphoma [13] and was the first compound approved by the Food and Drug Administration (FDA) for the treatment of hypercalcemia of malignant origin [14, 15]. Indeed, studies on the anti-tumor activity of gallium nitrate have shown a decrease in blood calcium concentration in patients treated with this agent. Given these results, research has been conducted to examine the potential activity of gallium nitrate for treating cancerous diseases associated with elevated blood calcium concentrations, such as hypercalcemia of malignant origin and osteoporosis. As bisphosphonates are the standard of care for these diseases, randomized clinical trials have been conducted to compare the efficacy of gallium nitrate versus etidronate and pamidronate in the treatment of hypercalcemia in patients with cancer. These trials showed that 82% of the patients treated with gallium nitrate had normal blood calcium levels compared to 43% of those treated with etidronate [16]. The second study showed that 69% of the patients treated with gallium nitrate had normal blood calcium levels compared to 56% of those treated with pamidronate [17]. A randomized double-blind comparative study of gallium nitrate and calcitonin (used in the treatment of hypercalcemia) for patients with moderate to severe hypercalcemia showed that 75% of the patients treated with gallium nitrate had normal blood calcium levels compared to 31% of those treated with calcitonin [18].

In addition to its ability to regulate blood calcium levels, gallium nitrate inhibits bone remodeling and reduces osteolysis in patients with multiple myeloma [19] and bone metastases [20]. Furthermore, the administration of low doses of gallium nitrate in patients with Paget's disease, a disease characterized by abnormal bone remodeling, reduces the hyperactivity of bone resorption [21, 22]. Additionally, the treatment of myeloma with gallium chemotherapy reduced bone loss and, consequently, pain. These studies have shown that gallium reduces the number of vertebral fractures, thereby prolonging the survival of these patients compared to conventional chemotherapy. However, the bioavailability of gallium nitrate is low and therefore requires a long and continuous IV administration to minimize its nephrotoxicity, hence, there is interest in the local release of gallium at the pathological site through an injectable CPC.

Typically, drugs can be included in CPCs by (i) mixing the drug powder with the solid phase, (ii) dissolving it in the liquid phase, and (iii) impregnating one of the CPC solid-phase components with a solution of the drug. Accordingly, three routes of gallium introduction were identified: (i) addition of gallium via the liquid phase, (ii) addition of gallium via salt or oxide in the powder mixture, and (iii) incorporation of gallium into one of the CPC solid-phase components by substitution with calcium. However, regardless of the route of introduction, it should be noted that there is sometimes a significant discrepancy between the properties of the cement and the surgeon's expectations [5].

An injectable CPC must be easy to prepare and homogeneous without phase separation during implantation. It must be cohesive, meaning that it does not disintegrate when in contact with biological fluids. The initial setting time of the cement should be short (4–8 min) but long enough to accommodate defects without damaging its microstructure. The initial mechanical properties of cement should be sufficiently high to decrease the patient's bedtime.

Concerning the preparation of gallium-filled cements, the introduction of various mass percentages of gallium oxide or nitrate into the solid phase of a commercial CPC did not allow the cement to set. Concerning the liquid phase, the introduction of gallium nitrate, which is not very soluble outside a very acidic pH, led to the formation of a gallium phosphate precipitate at physiological pH. Alternatively, it was shown that the introduction of gallium into one of the constituents of the solid phase of this cement did not significantly affect the main properties of the biomaterial, in terms of injectability and setting time [23, 24]. However, under *in vitro* conditions, the amount of gallium released from the obtained cement granules was found to be very low, due to the low initial loading rate (0.3 wt% of Ga) and complex speciation phenomena in the solution. However, it increases in the presence of osteoclastic cells [25]. As a matter of fact, gallium nitrate is currently considered the first generation of galliated compounds [26]. New second, and third-generation compounds are currently in clinical or pre-clinical trials to present greater efficacy and fewer side effects. Ligand-protected gallium (III) complexes represent the second generation of antineoplastic compounds [27–29]. Among them, gallium maltolate (GaM) has several advantages over gallium metal salts [30]. These include its better bioavailability, as the coordination of the ligands affects the speciation of gallium in the internal medium, increasing its effective



concentration, as well as its higher cytotoxicity than gallium nitrate in lymphoma cell lines. Gallium maltolate also inhibits the growth of lymphoma cells that are resistant or have acquired resistance to gallium nitrate, suggesting that the mechanisms of cytotoxicity are complementary to those of gallium nitrate [31].

Therefore, this article aims to propose the synthesis of new injectable CPCs containing a second-generation gallium compound, gallium maltolate. The physicochemical, rheological, and mechanical properties will be studied in comparison with those of the same unloaded cement already used in the clinic. Finally, the release of the active substance will be characterized.

2. Materials and methods

2.1. Gallium maltolate and gallium-loaded CPCs preparation

2.1.1. Synthesis of gallium maltolate (GaM)

The synthesis of gallium maltolate (figure 1) was based on Bernstein's report [32]. The complex was prepared by mixing aqueous solutions of maltol at 0.5 mol.l^{-1} (Sigma Aldrich) and gallium nitrate hydrate at 1 mol.l^{-1} ($\text{Ga}(\text{NO}_3)_3 \cdot x\text{H}_2\text{O}$, ACROS Organics) in proportions equivalent to a 3:1 molar ratio (maltol:gallium). Depending on the synthesis, values of x between 10 and 11 were determined beforehand using a DL38 volumetric Karl Fisher titrator. Subsequently, solid Na_2CO_3 was added slowly to obtain a final pH between 7 and 8 to achieve GaM precipitation. The solution was then heated at 65°C for two hours. The resulting precipitate was a white to pale beige crystalline powder. After cooling in an ice bath, the solid was filtered through a Millipore ($0.22 \mu\text{m}$ PTFE filter) and purified by successive washes with water and ethanol. Finally, the complex was heated to reflux in ethanol at 80°C , filtered, washed with ethanol, and dried. The final yield was 60%.

To confirm the purity of the product obtained, the following analyses were carried out: elemental analysis (C, H), ^1H and ^{13}C NMR, atomic absorption spectroscopy (AAS), UV-visible, pXRD, and FTIR. The obtained results from the different analyses agreed with previous publications [32, 33], and are given as supplementary data.

2.1.2. Synthesis of GaM-loaded cements

The cement formulations were prepared from a commercial apatite cement (Graftys[®] Quickset) whose phosphate solid phase, after MAS NMR ^{31}P analysis, was mainly composed of α -TCP ($\text{Ca}_3(\text{PO}_4)_2$, 60 wt%), mixed with anhydrous dicalcium phosphate [DCPA] (CaHPO_4 , 16.6 wt%), calcium deficient apatite [CDA] ($\text{Ca}_{10-x}[\text{HPO}_4]_y(\text{PO}_4)_{6-y}(\text{OH})_{2-z}$], 20.5 wt%), and dicalcium phosphate dihydrate [DCPD] ($\text{CaHPO}_4 \cdot 2\text{H}_2\text{O}$, 2.8 wt%). The gallium maltolate complex was directly added as a powder to the solid phase at 3.5 and 7% w/w. The mixtures were subsequently homogenized using a three-dimensional stirrer for one hour at a speed of 50 rpm. After this step, the cement paste was prepared by mixing the powder with a 0.5 wt% Na_2HPO_4 hardener solution with a liquid-to-powder ratio of $L/P = 0.45$. CPCs were referenced according to the following denominations:

- CPC-Ctrl for the control cement,
- CPC-3.5G for the formulation of a combined cement with 3.5 wt% of GaM,
- CPC-7G for the formulation of a combined cement with 7 wt% of GaM.

2.2. X-ray powder diffraction (pXRD)

The diffraction patterns (GaM and CPCs) were recorded using a D8 Advance diffractometer (Bragg-Brentano type geometry in theta/2theta mode) with an x-ray tube equipped with a copper anode. The diffractometer had a

Ge front monochromator thus allowing the selection of Cu $K\alpha_1$ radiation ($\lambda = 0.1540593$ nm). The silicon detector collects x-rays simultaneously with a workable angle range of 0.5 to $150^\circ 2\theta$. The measurements were carried out under the following conditions: x-ray tube with 40 kV voltage and 40 mA current, one hour for each diagram ranging from 5° to $60^\circ 2\theta$ with a pitch of $0.1^\circ 2\theta$.

2.3. Fourier transform infrared (FTIR) spectroscopy

Fourier transform infrared (FTIR) spectra were recorded using an FTIR spectrometer (Bruker Tensor 27). The measurements (GaM and CPCs) were made from KBr pellets with a ratio of 100 mg of anhydrous KBr to 1 mg of the sample. Each acquisition was recorded under dry purified atmosphere in a spectral range of 4000 to 400 cm^{-1} with 128 scans and a spectral resolution of 2 cm^{-1} .

2.4. Atomic absorption spectroscopy (AAS)

A calibration range (established between 1 and 100 ppm) was first prepared from a standard solution of gallium nitrate for AAS at 1000 ppm (Sigma Aldrich). Measurements were performed on an iCE™ 3300 AAS Atomic Absorption Spectrometer. The experimental conditions for this device were as follows: a wavelength of 287.5 nm, an air/acetylene flame, a flow rate of 1.2 $\text{ml}\cdot\text{min}^{-1}$, and a burner height of 12.4 mm.

2.5. ^1H and ^{13}C nuclear magnetic resonance (NMR)

^1H and ^{13}C NMR spectra were recorded on a Bruker Avance 300 spectrometer fitted with a 5 mm BBO probe tuned to a recording frequency of 300.13 MHz (for ^1H) and 75.47 MHz (for ^{13}C), and the temperature of the probe was set at room temperature (approximately 294 K).

The spectra are referenced to the DMSO (2.54 ppm for ^1H NMR and 39.51 ppm for ^{13}C NMR).

Chemical shifts (data given in ppm) and coupling constants (J) are given in Hz with the following splitting abbreviations: s singlet, d doublet.

2.6. ^{31}P and ^{71}Ga MAS NMR

To characterize the final phosphorous species composition of the cement, high-resolution solid-state magic-angle spinning (MAS) NMR was performed before and after association with the gallium complex. ^{31}P NMR experiments were conducted on a 300 MHz Bruker Avance II spectrometer operating at 7 T (^1H and ^{31}P Larmor frequencies of 300 and 121.5 MHz respectively) using a 4 mm double resonance MAS probe and a spinning rate of 12 kHz.

For all experiments, ^1H SPINAL-64 [34] (RF field strength of 70 kHz) was applied during signal acquisition. Quantitative ^{31}P MAS spectra were recorded using a 24° flip angle (pulse length of 1 μs), and 64 scans were accumulated with a recycle delay of 60 s ensuring complete relaxation of the magnetization. ^{31}P chemical shifts were referenced relative to 85% H_3PO_4 .

To follow *ex situ* the gradual transformation of α -TCP into CDA, the quantitative ^{31}P MAS spectra were deconvoluted using the dmfit program [35] using several independent contributions. The relative amount (wt%) of each phase as a function of setting time was determined by assuming that the composition of the CDA phase formed was close to that of $\text{Ca}_9(\text{HPO}_4)(\text{PO}_4)_5\text{OH}$.

To check the structural integrity of the gallium complex, solid-state NMR analyses of gallium were performed before and after its association with CPC. ^{71}Ga NMR experiments were performed on an 850 MHz Bruker Avance III spectrometer ($B_0 = 20$ T, ^{71}Ga Larmor frequency of 259.3 MHz) using a 1.3 mm double resonance MAS probe. The ^{71}Ga central transition (CT)-selective MAS spectra were recorded using a Hahn echo sequence with whole echo acquisition. The echo delay was synchronized with the rotor period, and the RF-field strength was 62.5 kHz, corresponding to a CT-selective $\pi/2$ pulse of 2.1 μs . More than 200,000 scans were accumulated with a 1 s recycling delay. The ^{71}Ga chemical shifts were referenced relative to 1 $\text{mol}\cdot\text{l}^{-1}$ $\text{Ga}(\text{NO}_3)_3$ solution. The ^{71}Ga MAS spectra were deconvoluted using the dmfit program [35] using line shapes characteristic of quadrupolar interactions defined by an isotropic chemical shift (δ_{iso}), quadrupolar coupling constant (C_Q), and asymmetry parameter (η_Q).

2.7. Scanning electron microscopy (SEM)

Samples were prepared either from a fracture of a cylinder of CPC using a cutter or from a polished cross-section using a JEOL cross-section polisher SM09010 by applying an argon ion beam accelerated by a voltage up to 6 kV perpendicular to the surface of each specimen (1 mm^2) for 6 h. SEM observations of those samples were performed using a Field Emission Gun Scanning Electron Microscope (Jeol 7600F). Images were acquired in the backscattered electron mode with a 9 pA beam current and 10 kV accelerated voltage.

2.8. Raman mapping

Acquisition was performed using a Raman Renishaw InViaTM spectrometer whose microscope is equipped with an automated micrometric XY plate for sample mapping. The settings used for this analysis were as follows: laser wavelength 785 nm, power 50 mW, objective $\times 20$, and exposure time 5 s.

The samples ($N = 6$) used were cylinders of GaM-loaded CPC (internal diameter: 6 mm, height: 12 mm). After drying for 30 min at room temperature, each cylinder was demolded, weighed, and immediately immersed in saline solution according to the release protocol. To map the cylinders at different release times, the saline solution was completely removed, and the samples were placed in an oven at 37 °C. The release times used for mapping were $t = 0, 1, 24, 72,$ and 192 h. The cylinders were broken into two parts using a cutter. After a preview of the analyzable surface of the sample, rectangular mapping was performed on a surface with a length of 6000 μm and a width of 1500 μm using an x and y pitch of 150 μm . The total time required for each mapping was 41 min.

2.9. Determination of mechanical properties

2.9.1. Setting time

The setting times were determined using a standard method: the Gillmore needle method (ASTM C266–20) [36]. This method allows the setting speed of cement to be estimated visually. The device consists of a needle measuring the initial setting time noted t_i (diameter: 2.12 mm, weight: 113.4 g). In practice, the cement paste is placed in a cell (cylindrical shape, internal diameter: 20 mm, depth: 4.7 mm) thermostated at 37 °C. The measurement was then performed by gently placing the needle on the surface of the cement. The latter is then subjected to the pressure of the needle (0.3 MPa), which leaves indentation marks at the beginning of the reaction that diminish over time. The measurement was collected when the indentations were no longer visible.

2.9.2. Injectability and workability

The injectability was measured using an Advanced Material Testing System texture analyzer (AmetekLS5) equipped with a syringe holder. The test consisted of measuring the force required to extrude the cement paste from a syringe. Specifically, after mixing the solid and liquid phases of the cement for 30 s, the paste was transferred into a syringe with a filling time of approximately 1 min 30. For these tests, the syringes used are Terumo[®] syringes (2.5 ml), double-bevel outlet, internal surface 64 mm², and an outlet section of 1.6 mm (i.e., 14 G). Then, the syringe was placed on the support, and injectability was measured 3 min after the beginning of the mixing. The time chosen for injectability is the minimum time to perform all the steps previously described, and it conforms to the recommendations of the industry that recommends injecting the cement after 2 min of mixing. The displacement speed imposed on the piston for extrusion was 1 mm.s⁻¹. At the end of the measurement, the extruded paste was visually checked to ensure that the measurement was not affected by the demixing phenomenon. Three trials were conducted for each cement composition. The percentage of extruded paste for each trial was calculated by weighing the syringe before filling, after filling, and at the end of the cement paste extrusion.

To complete this study, the workability of CPCs was studied by making successive extrusion measurements at different times. Specifically, injectability measurements were performed at 3, 5, and 8 min following a previously described protocol. These experiments allow the comparison of the setting speed and provide information on the time at which the product can be operated and injected.

2.9.3. Compressive strength

Compressive force measurements were performed using an Advanced Material Testing System texture analyzer (AmetekLS5). This device measures the deformation of the material as a function of compressive force (ASTM C39M-21) [37]. The tests consisted of subjecting a cement cylinder to an axial force by placing it on a platform located under a flat piston attached to the measuring cell. For this purpose, the cement cylinders are prepared using polytetrafluoroethylene (PTFE) molds with an internal diameter of 6 mm and a height of 12 mm. After 30 min of drying at room temperature, the molds were immersed in an isotonic NaCl solution (9 wt%) for 72 h to mimic the setting of the cement in a biological environment. Once set, the cylinder was placed at the center of the platform. A speed of 1 mm.s⁻¹ is then imposed on the piston over a distance of 6 mm. The compressive strength was calculated from the measured maximum force ($N = 3$).

2.9.4. Porosity

The porosity of each formulation was calculated from the cement specimens prepared according to the method described in the previous paragraph. Once the cylinders were removed, they were weighed and measured. The equipment used was a helium pycnometer AccuPyc II 1340 Micromeritics with a measuring cell of 1 cm³ and a

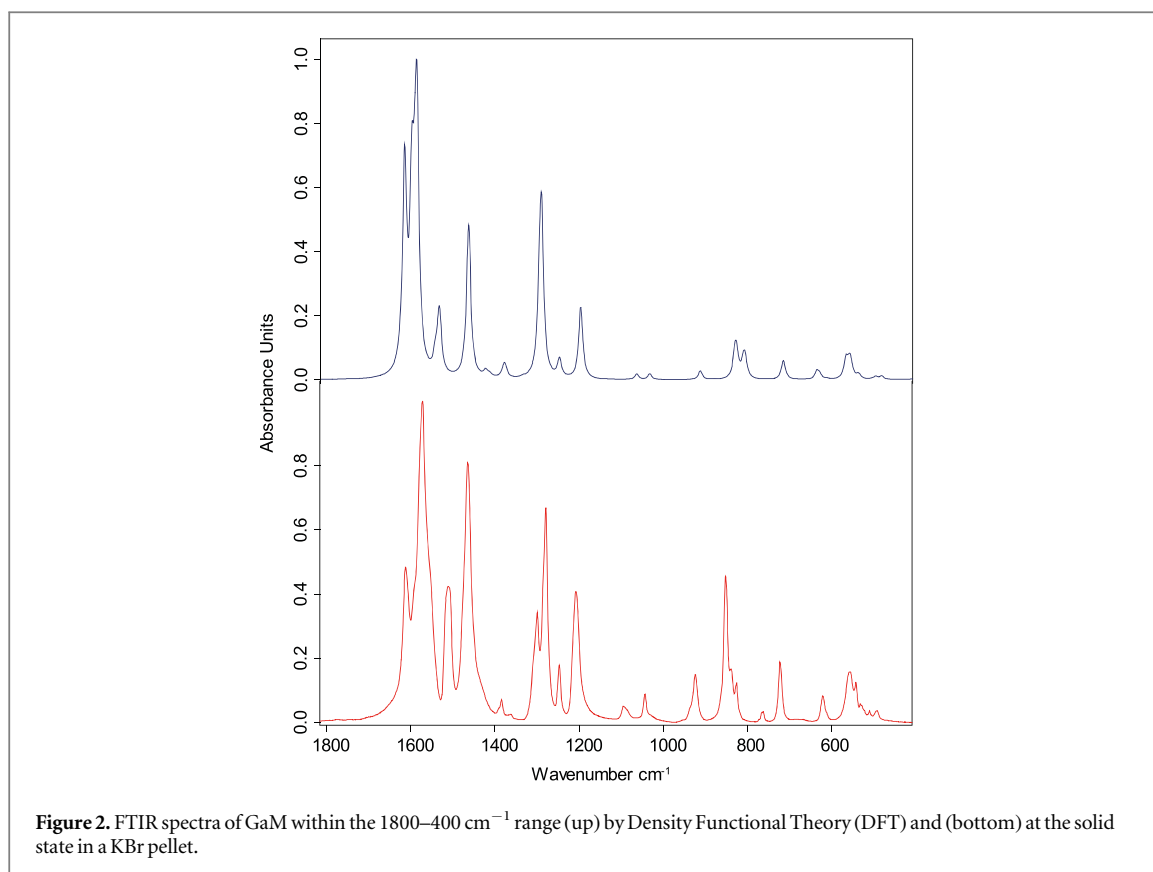


Figure 2. FTIR spectra of GaM within the 1800–400 cm^{-1} range (up) by Density Functional Theory (DFT) and (bottom) at the solid state in a KBr pellet.

calibration ball with a theoretical volume of 0.718502 cm^3 . Once the sample was inserted into the measuring cell, the acquisition was launched. The measurement was validated when $\sigma \leq 0.01\%$ for the last five values.

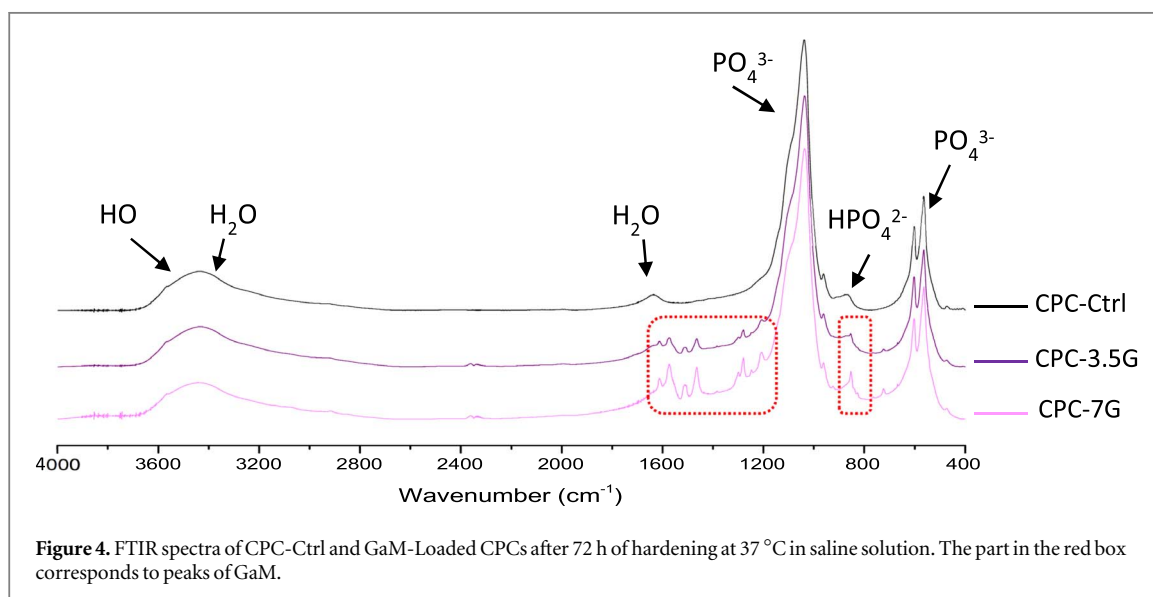
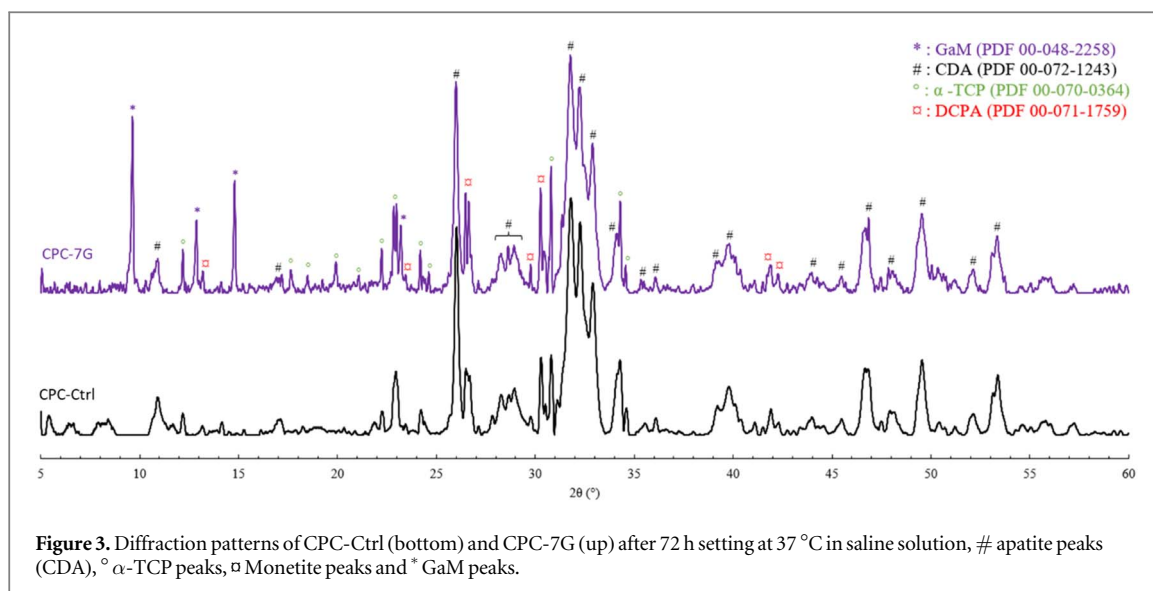
3. Results and discussion

3.1. GaM: analysis of FTIR spectra, a theoretical approach

Attributions of the main absorption vibrational bands of gallium maltolate were provided in these studies [32, 33] with $\nu_{\text{arom CH}}$ stretching vibration at 3070 cm^{-1} , $\nu_{\text{aliph CH}}$ stretching vibration at 2910 cm^{-1} , $\nu_{\text{C=C}}$ stretching vibration at 1612 cm^{-1} , and $\nu_{\text{C=O}}$ stretching vibration at 1572 cm^{-1} . However, the last two absorption bands were inversely assigned in a third publication [38]. Indeed, redshifts of $\sim 50 \text{ cm}^{-1}$ relative to both the $\nu_{\text{C=O}}$ and $\nu_{\text{C=C}}$ stretching vibrations of the free ligand are attributed to the influence of the coordination of the maltol with a metal ion through its carbonyl group oxygen atom. To clarify the assignment of the $\nu_{\text{C=O}}$ and $\nu_{\text{C=C}}$ stretching vibration bands, the theoretical infrared spectrum of GaM was computed within the Density Functional Theory formalism. The crystalline structure of GaM, listed within the Cambridge Structural Database (CSD) [39] with the GUYBAD refcode [32], has been used as the starting geometry for structure optimization in the gas phase. This geometry optimization was performed using the Gaussian09 program [40], the M06–2X functional [41], and the 6–31 + G(d,p) basis set. The harmonic vibrational frequencies were evaluated to allow the assignment of the absorption bands and to confirm the structure as an energetic minimum (absence of imaginary frequency). As illustrated in figure 2, a good qualitative agreement was obtained between the experimental and theoretical infrared spectra after the application of the recommended scaling factor (0.952) to the computed vibration bands [42]. Visualization of the vibrational motions using the GaussView software reveals that most of the absorption bands observed experimentally are not pure modes, but rather combinations of two, or more, modes of vibration. Hence, the two bands at 1612 and 1572 cm^{-1} can neither be assigned to pure $\nu_{\text{C=O}}$ or $\nu_{\text{C=C}}$ stretching vibrations as previously assigned, but to the coupling of these two oscillators.

3.2. Characterization of CPCs loaded with GaM

The nature of the final product obtained from each cement formulation was studied using powder x-ray diffraction (pXRD), infrared spectroscopy (FTIR), and ^{31}P solid-state MAS NMR.



3.2.1. Powder x-ray diffraction (pXRD)

The diffraction patterns (figure 3) of the control CPC and CPC-7G were similar to the lines representing CDA, α -TCP, and DCPA. The observation of CDA in distinct types of cement proves that a hydrolysis reaction occurred. Additionally, the α -TCP lines indicate that the reaction is not complete, and that its level of advancement does not seem to have been modified by the addition of the gallium complex. It is also possible to observe on the diffraction pattern of CPC-7G, the lines corresponding to GaM at 9.56, 12.89, 14.73, and 23.12 ° 2 θ , indicating that the complex is still present after 72 h in the NaCl solution.

3.2.2. Fourier transform infrared (FTIR) spectroscopy

The FTIR analysis (figure 4) also confirmed the presence of CDA after the setting process for CPC-Ctrl and the CPCs loaded with GaM (3.5 and 7 wt%). We can observe bands representing the water in the ranges 3500–3000 cm^{-1} and 1700–1600 cm^{-1} , those representing the vibrations of the PO_4^{3-} groups located in the ranges 1200–950 cm^{-1} and 650–500 cm^{-1} , and those representing vibrations of the HPO_4^{2-} groups of apatite in the range 900–800 cm^{-1} and finally, the hydroxyl group band of hydroxyapatite at $\sim 3570 \text{ cm}^{-1}$. The GaM bands were also observed in each spectrum of GaM-loaded CPCs in the range 1700–1200 cm^{-1} and $\sim 900 \text{ cm}^{-1}$. These bands represent carbonyl group vibrations, C=C double bonds, and CH bonds, respectively. These locations are in agreement with the FTIR spectrum of the pure GaM complex.

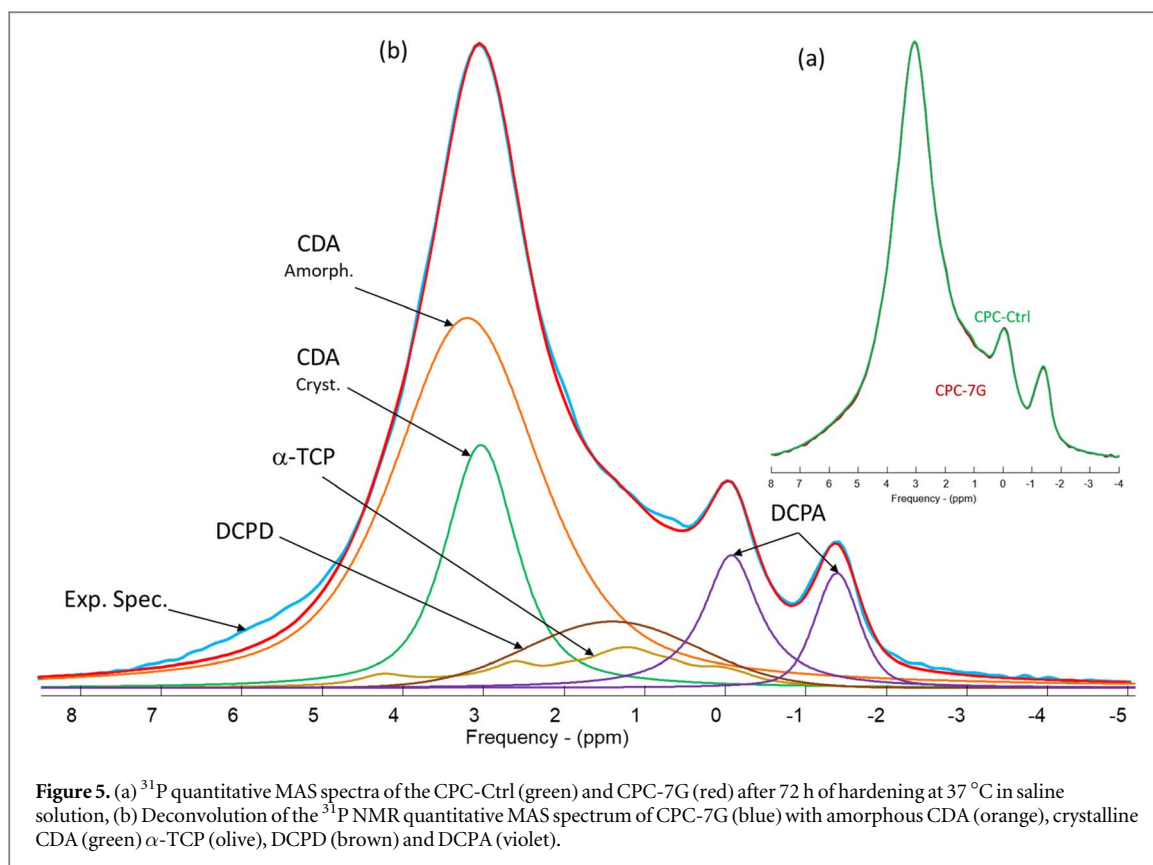


Figure 5. (a) ^{31}P quantitative MAS spectra of the CPC-Ctrl (green) and CPC-7G (red) after 72 h of hardening at 37 °C in saline solution, (b) Deconvolution of the ^{31}P NMR quantitative MAS spectrum of CPC-7G (blue) with amorphous CDA (orange), crystalline CDA (green) α -TCP (olive), DCPD (brown) and DCPA (violet).

Table 1. pXRD and NMR analysis of CPC-Ctrl and CPC-7G components after 72 h setting at 37 °C in saline solution.

Samples	CPC powder ^{31}P MAS NMR	CPC-Ctrl		CPC-7G	
		pXRD	^{31}P MAS NMR	pXRD	^{31}P MAS NMR
α -TCP (PDF 00-070-0364)	60.0	43	1.8	47.6	6.6
Crystalline CDA (PDF 00-072-1243)	8.3	38.3	29.8	33.1	17.8
Amorphous CDA	12.2	—	48.4	—	52.8
DCPA (PDF 00-071-1759)	16.6	18.7	10.9	19.3	13.5
GaM (PDF 00-048-1511)	—	—	—	5%	—
DCPD	2.8	—	9.1	—	9.2
Total (%)	99.9	100	100	95–100	99.9
α -TCP conversion rate (%) ^a	—	37.1	93.8	30.4	74.5

^a Calculations were made considering the crystallized species.

3.2.3. ^{31}P MAS NMR

Figure 5(a) shows a comparison of ^{31}P quantitative MAS NMR spectra of the two types of cement: control (CPC-Ctrl) and GaM-loaded cement (CPC-7G). The spectra were almost identical. The deconvolution of the spectra is shown in figure 5(b).

The contribution of α -TCP was obtained from the spectrum of the pure compound with its amplitude remaining free during the simulation. All other signals are Lorentzian lines centered (in ppm) at -1.4 and -0.1 for DCPA, 1.4 for DCPD, 3 and 3.2 for crystalline and amorphous CDA, respectively. The weight percentage of CDA for 72 h hardened CPC-Ctrl and CPC-7G cements was estimated to be approximately 78 wt% and 71 wt% respectively, indicating that the addition of gallium maltolate marginally affects the transformation rate of α -TCP into CDA.

Solid-state MAS NMR has the advantage of being able to analyse the phases obtained during the setting of the cement, regardless of their crystallinity. Table 1 highlights this result because the conversion rate of α -TCP is more than doubled compared to the results obtained by QUALX on pXRD data. Interestingly, QUALX software estimates the amount of the different phases in the compound by determining the intensity ratio of the most intense diffraction peaks of each species [43]. Additionally, whether any such analysis will estimate the proportions of the species in a compound, and even using a more efficient Rietveld refinement method, the

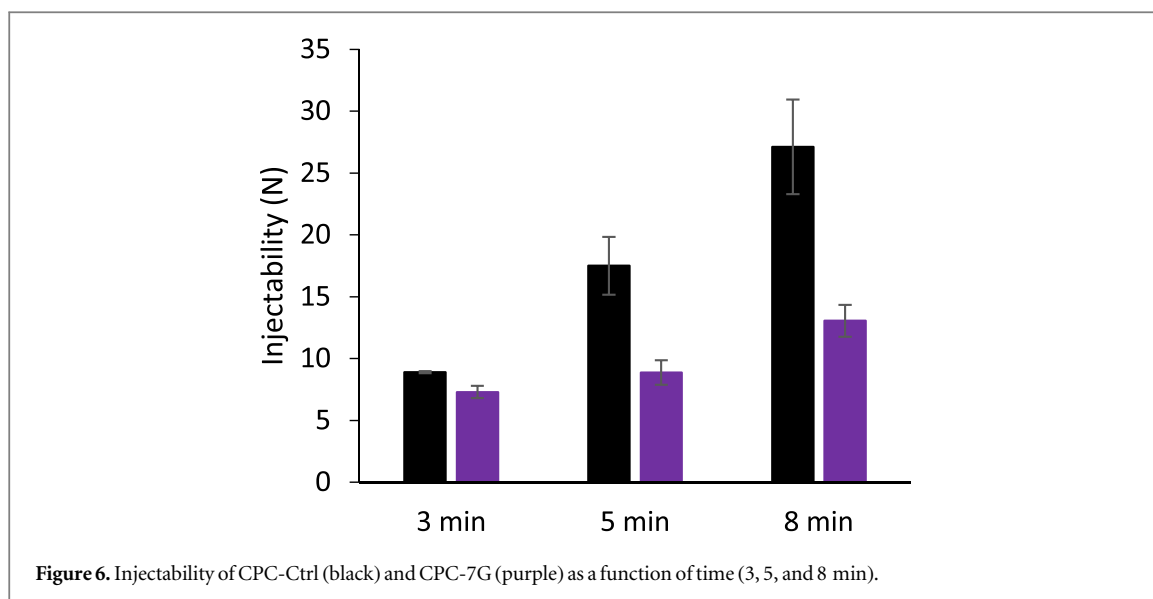


Table 2. Summary of the textural properties of GaM-loaded formulations.

Sample	CPC-Ctrl	CPC-3.5G	CPC-7G
L/P ratio	0.45	0.45	0.45
t_i (min)	5.30–6	5.30–6	5–5.30
Injectability after 3 min (N)	10.4 ± 0.2	6.6 ± 0.1	6.5 ± 0.1
Cohesiveness	Very good	Excellent	Excellent

pXRD data will only give information concerning the crystallized species and the transformation rates will be systematically lower than those obtained using NMR MAS analysis [44–46]. Concretely, the same observations can be made for injectable CPCs by comparing the results obtained by complex impedance, NMR MAS, and pXRD [47, 48].

3.3. Textural properties of GaM-loaded cements

Textural properties are essential for injectable cement. Parameters, such as setting time, injectability, workability, and cohesiveness, were studied (table 2) according to the protocols described in the experimental section. Thus, the setting times obtained are respectively from 5.30 to 6 min for the CPC-Ctrl and the CPC-3.5G and from 5 to 5.30 min for the CPC-7G. There was no significant difference between the setting times of the GaM-loaded CPCs and CPC-Ctrl.

To manually inject the different formulations, injectability tests were performed. The results show a difference between CPC-Ctrl and GaM-loaded CPCs, with the latter being more injectable.

Theoretically, an increase in the grain size, as shown in figure 9 (see *infra*), leads to a decrease in injectability [5], whereas our tests show an increase in this parameter.

At present, our only hypothesis is that this change originates from the maltol ligand. However, no study has mentioned the rheofluidifying properties of maltol because the latter is used either as a taste enhancer [49] or to increase the bioavailability of certain metals such as iron, aluminium, or gallium [32, 50, 51]. Additionally, the injectability between the two GaM-loaded CPCs was not affected by the proportion of GaM. Workability was studied at an average temperature of 26 ± 1 °C. Under these conditions, commercial CPC (CPC-Ctrl) had a setting time of 8 min. The injectability of the CPC-Ctrl (figure 6) decreased over time; this being consistent with the setting time of the latter (8 min). The addition of GaM prolonged the injectability of the cement to 8 min. At this time, the injectability of the latter is 13.1 ± 1.3 N and is below the limit of manual injectability (the maximum value for conventional ancillaries having been arbitrarily set at 25 N).

As illustrated in figure 7, injectability profiles of CPC-Ctrl and GaM - containing formulations (CPC-3.5G and CPC-7G) reflected fully injectable cement pastes behavior [5, 52]. In relation with the calculated injectability forces (table 2), the use of GaM enhances the extrusion (horizontal plateau). Moreover, all of the cement pastes were fully extruded with a percentage higher than 95%.

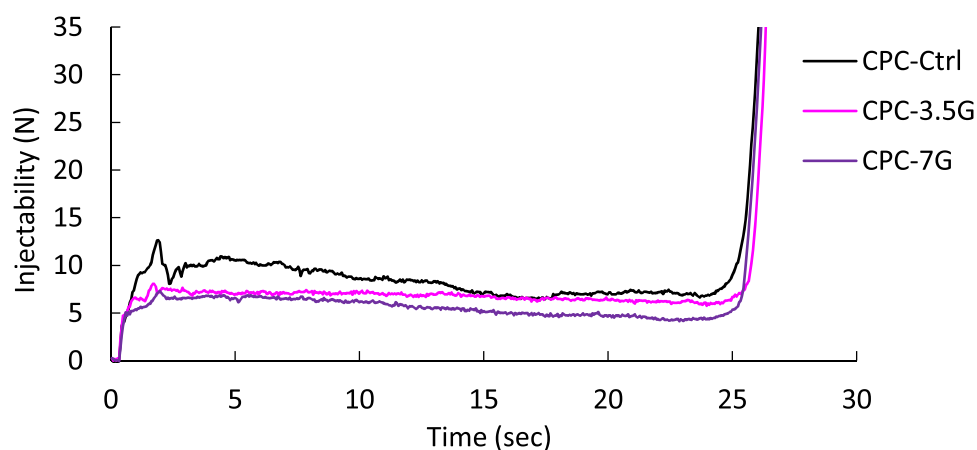


Figure 7. Injectability profiles of CPC-Ctrl (black), CPC-3.5G (pink), and CPC-7G (purple) after 3 min hardening at room temperature.

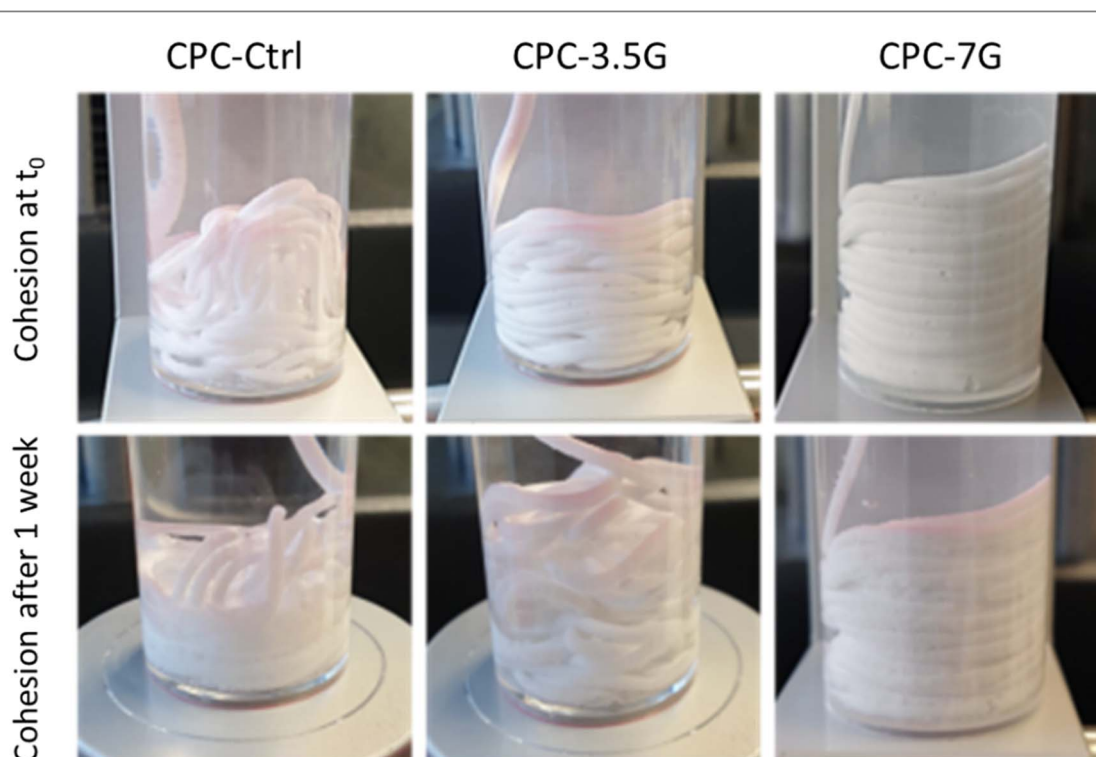


Figure 8. Cohesion of extruded CPC-Ctrl, CPC-3.5G and CPC-7G pastes after setting at 37 °C in a 0.9 wt% NaCl solution.

The cohesion of the GaM-loaded CPCs was also visually checked (i) immediately (t_0) after their immersion in a NaCl solution and (ii) after one week of setting in the same solution stored at 37 °C (figure 8). Visual examination showed no fundamental differences between the CPCs that remained cohesive.

3.4. Influence of gallium maltolate on the structure of the biomaterial

Firstly, the porosity studied by helium pycnometry gave a value of about 50% for CPC-Ctrl and CPC-7G and 47% for CPC-3.5G. Nevertheless, this difference is not significant.

Figure 9 shows the microstructure of the different GaM-loaded CPC formulations compared with that of the CPC-Ctrl after 72 h of saline treatment. At low magnification (figure 9(a)), a clear fracture was observed for the three materials, indicating their fragility. The surface was smooth for all samples and contained air bubbles trapped during cement mixing and setting, with diameters ranging from 30 to 100 μm . Nevertheless, it appears that in the CPC-3.5G image, the diameter of the bubbles is larger (30–150 μm), but this is not associated with a slightly higher porosity. At a higher magnification (figure 9(b)), the same specificities were observed between the

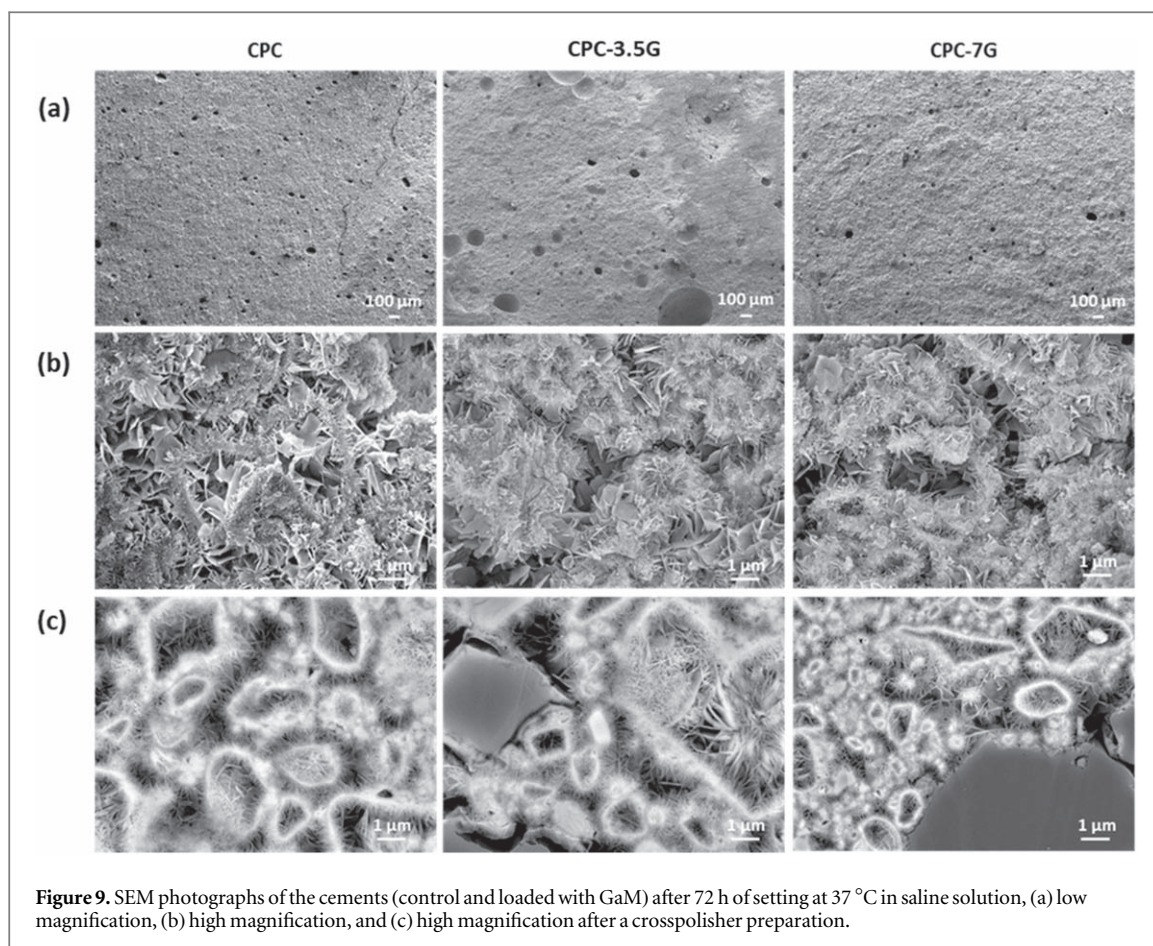


Figure 9. SEM photographs of the cements (control and loaded with GaM) after 72 h of setting at 37 °C in saline solution, (a) low magnification, (b) high magnification, and (c) high magnification after a crosspolisher preparation.

GaM-loaded CPCs and the CPC-Ctrl. In addition, we found geodes characteristic of the hydrolysis of α -TCP as well as the entanglement of apatitic crystals, which seem identical in the three types of CPCs. The crosspolisher preparation presented in figure 9(c) makes it possible to highlight these observations as well as the interface between the GaM powder and cement.

The GaM-loaded CPCs (figure 10(a)) have a mechanical strength (26.6 ± 1.3 and 26.8 ± 0.5 MPa for the CPC-3.5G and CPC-7G respectively) significantly lower than that of CPC-Ctrl (31.1 ± 0.3 MPa). In addition, the shape of the compressive strength curves (figure 10(b)) shows a clear break at the top, which is typical for brittle materials.

Considering the measured porosity values for CPC-Ctrl, CPC-3.5G and CPC-7G, they cannot entirely explain a decrease in mechanical strengths of GaM-loaded CPCs.

We hypothesize that this decrease is due to other factors such as an interaction between the gallium maltolate complex and the CPC interfering with the crystallogenes process, or also the trapping of GaM grains that causes preferential fractures in the material. Even if the last assumption is most likely, we have highlighted (table 1) that the conversion rate of α -TCP into CDA seems to be a little lower in the case of the CPC-7G than the CPC-Ctrl.

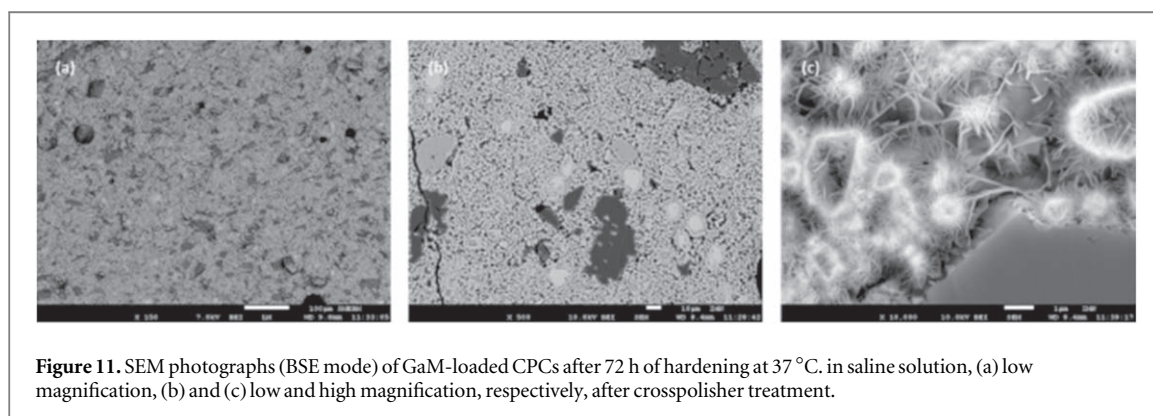
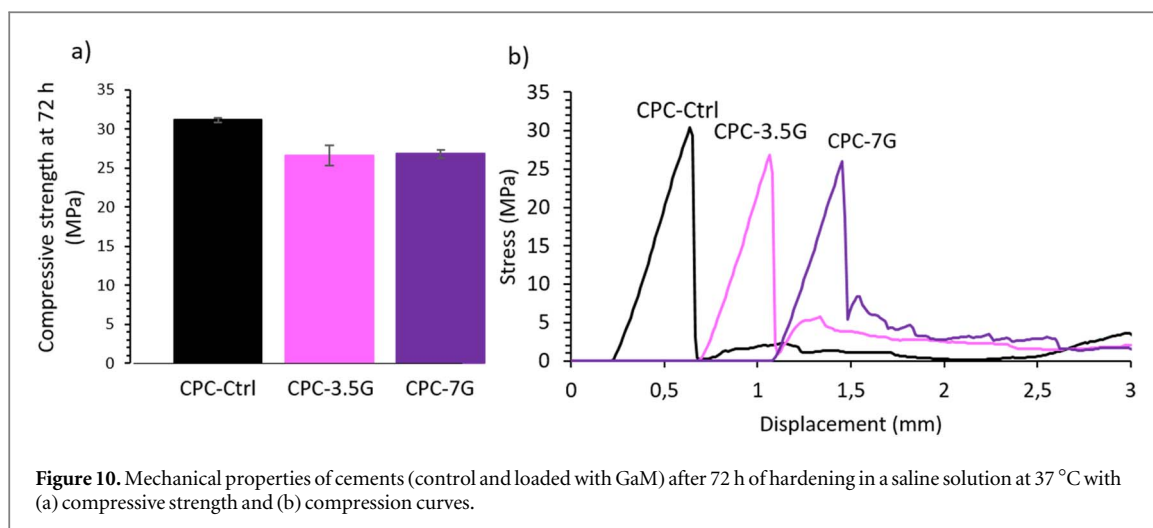
This decrease in the transformation rate could reduce the apatite crystals entanglement in a three-dimensional space, inevitably resulting in a lowering in mechanical resistance. Despite that the mechanical resistances are reduced, the CPC-7G formulation meets regulatory and user requirements.

Indeed, concerning a non-weight-bearing intraosseous indication, injectable α -TCP based CPCs have compressive strengths comparable to those reported for human cancellous bone (4–12 MPa), [53] and are generally between 0.5 and 50 MPa [46, 54].

Therefore, the incorporation of GaM into Graftys products will not modify the actuals clinical biomechanical results [55, 56].

3.5. Integrity of gallium maltolate in cement

SEM images allowed us to study the morphology of the complex after its integration. The GaM powder consists of grains of inhomogeneous shape and size (ranging from a few microns to 10 microns). CPC-7G (figure 11(a)) shows a homogeneous distribution of GaM, which differs owing to the contrast imposed by the acquisition



mode (BSE). Here, gallium is surrounded by an organic ligand, and the latter is less rich in electrons compared than the CPC and therefore is darker. In addition, after integration, the size of the GaM grains was not modified, which indicates the good integrity of the complex within the CPC (figure 11(b)). Finally, at a high magnification (figure 11(c)), the GaM grains were fully integrated and trapped within the biomaterial. No change in the morphology of GaM was observed.

The SEM photographs show only the organic part of the complex, and energy-dispersive x-ray (EDX) mapping was performed to observe gallium. Mapping was conducted on a fracture of CPC-7G (figure 12(a)) covered with a thin layer of carbon. The mapping of gallium (figure 12(d)) is complementary to that of phosphorus and calcium (figures 12(b) and (c)). Phosphorus and calcium are present over the entire surface, except where gallium is present. This analysis confirmed that GaM was homogeneously distributed in the CPC.

To check the structural integrity of the GaM complex, solid-state NMR analyses of gallium were performed before and after association with CPC. GaM-loaded CPCs were prepared according to two different hardening processes: (i) immersion for 72 h in saline solution at 37 °C and (ii) placing in an oven at 37 °C whose atmosphere was saturated with water. The goal was to study the potential changes from both the mixture with the hardening liquid during the cement mixing stage and those resulting from the percolation of the NaCl solution. Figure 13 shows the ^{71}Ga NMR spectrum of GaM, as well as the GaM-loaded CPCs, charged at 7 wt% (CPC-7G) placed in a water-saturated oven or immersed in NaCl. These three spectra are similar in all respects, indicating that the gallium complex does not undergo major modifications (i) in spite of the hardening liquid during the mixing step or (ii) of the percolation of the saline solution during 72 h of setting. These results are consistent with the SEM observations.

The GaM ^{71}Ga NMR spectrum can be simulated (figure 13(d)) using a unique quadrupolar lineshape characterized by an isotropic chemical shift, $\delta_{\text{iso}} = 98.4$ ppm, quadrupolar coupling constant, $C_Q = 13.28$ MHz, and an asymmetry parameter, $\eta_Q = 0.8$. The gallium chemical shift is mainly influenced by its close oxygen surroundings but also by the nature of the atoms in the second sphere of coordination [57]. There is little data in the literature on gallium complexes, nevertheless, the observed ^{71}Ga is coherent with hexacoordinated

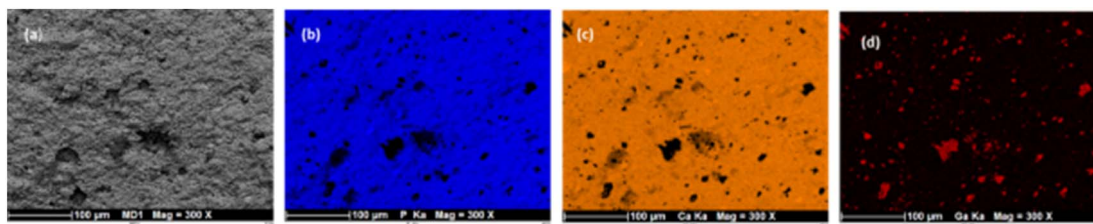


Figure 12. Elemental mapping of a CPC-7G (a) after 72 h of hardening at 37 °C in saline solution (b) phosphorus (blue), (c) calcium (yellow), and (d) gallium (red).

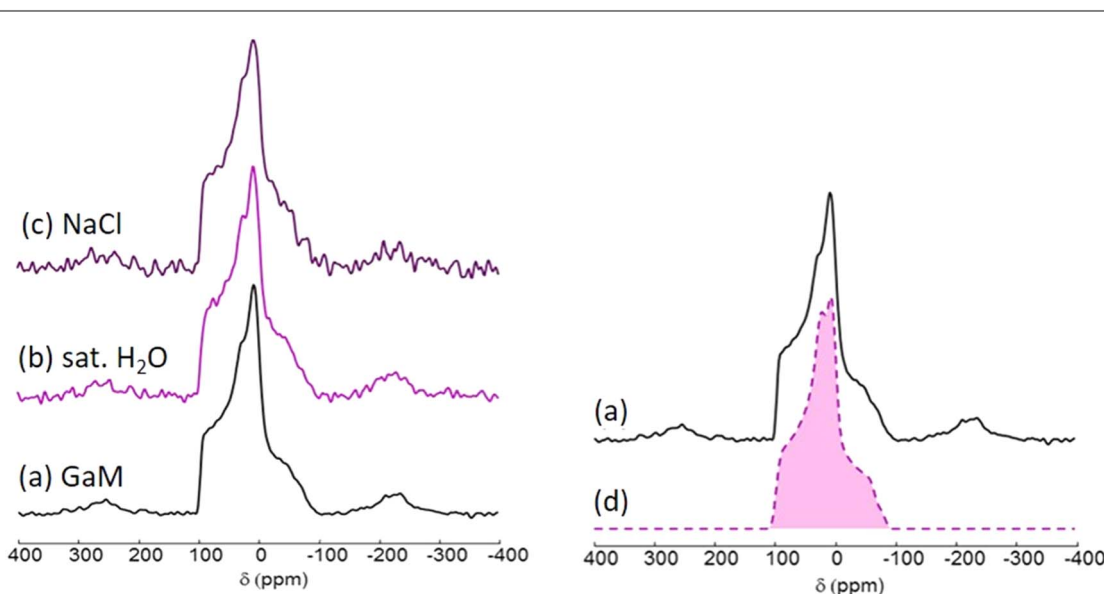


Figure 13. MAS ^{71}Ga NMR spectra (a) of pure GaM, CPC-7G after 72 h of setting at 37 °C (b) in water-saturated oven, (c) immersed in NaCl, (d) simulated.

gallium complexed with three maltolate ligands [58]. This structure is maintained whether the cement is placed in a water-saturated oven or immersed in NaCl.

3.6. *In vitro* studies of the release of gallium maltolate

A quantity (1.2 g) of cement was used (3.5 and 7 wt% GaM concentrations and an L/P ratio of 0.45) to form three pellets. After setting for 20 min at room temperature, the pellets were unmolded, weighed, and immersed in a saline solution (NaCl 0.9% w/w, 10 ml). They were placed on an orbital shaker (90 rpm) at 37 °C. Samples of 6 ml of the solution were collected regularly while the experiment was running and immediately replenished with a fresh solution. The sampled solutions were then filtered (PTFE, 0.45 μm) to eliminate potential cement particles that could alter the measurements. The released gallium was analysed by AAS, and the released GaM complex was studied by UV-visible spectrometry. All experiments were performed in triplicates.

The curves obtained (AAS) for CPC-3.5G and CPC-7G are shown in figure 14(a). Two distinct stages were observed: (i) a flash release for 8 h, in which 34 ± 1 and $28 \pm 1\%$ gallium was released from CPC-3.5G and CPC-7G respectively, and (ii) a gradually increasing release to a level of $49 \pm 1\%$ at 60 days for CPC-3.5G and $58 \pm 2\%$ at 116 days for CPC-7G. The UV spectrometry study (figure 14(b)) at the GaM complex wavelength (306 nm) for the two formulations showed the same characteristics with a release of $46 \pm 1\%$ at 60 days for CPC-3.5G and $60 \pm 2\%$ at 116 days for CPC-7G. Therefore, it can be concluded that during the study period, gallium was released as gallium maltolate.

At the end of the releases, the cement pellets were dissolved in a 5% HCl solution, and the remaining gallium was measured. Thus, thanks to this last measurement, we find $94 \pm 2\%$ of gallium initially present in the two cement formulations.

To identify the mechanisms involved in the release of the gallium from the cement, the release data (AAS) were analyzed using Higuchi [59], Korsmeyer-Peppas [60], and Kopcha [61] models (table 3).

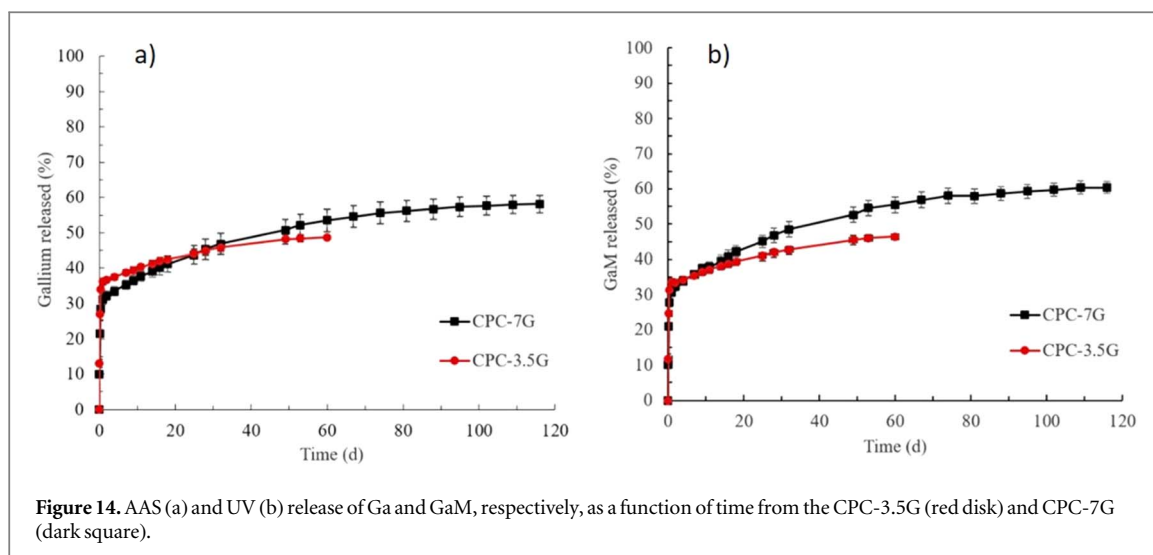


Figure 14. AAS (a) and UV (b) release of Ga and GaM, respectively, as a function of time from the CPC-3.5G (red disk) and CPC-7G (dark square).

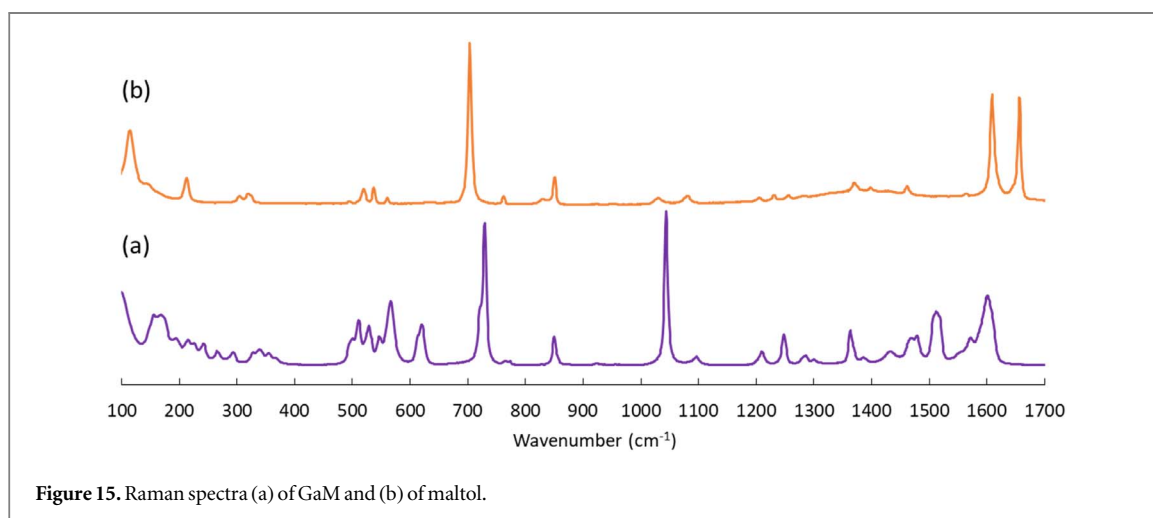


Figure 15. Raman spectra (a) of GaM and (b) of maltol.

Table 3. Parameters of the gallium release profile fitting, according to different models.

Sample	CPC-3.5G		CPC-7G	
	1	2	1	2
Drug release phase	1	2	1	2
Time (d)	0–0.3	0.3–60	0–0.3	0.3–116
Higuchi R ² coefficient	0.992	0.992	0.997	0.984
Higuchi Rate (%/d ^{1/2})	60	2	50.2	3
Korsmeyer-Peppas R ² coefficient	0.989	0.924	0.994	0.956
Korsmeyer-Peppas n	0.47	0.08	0.52	0.16
Sample	CPC-3.5G	CPC-7G		
Kopcha R ² coefficient	0.990	0.990		
Kopcha A/B	4.5	6.2		

The best results were obtained using the Higuchi model and confirmed by Kopcha, which indicates a mainly Fickian-diffusion mechanism [62, 63]. Nevertheless, it was possible to assume that the flash release came mainly from the ends of the cylinder owing to the greater accessibility of GaM to the fluids. To confirm this hypothesis, Raman mapping was performed for several samples. The CPC-7G formulation was selected for this experiment. Thus, the samples ($N = 6$) were mapped at different release times, which are $t = 0, 1, 24, 48, 72,$ and 192 h. The main bands used to localize GaM (figure 15(a)) and Maltol (figure 15(b)) were located at 729 cm^{-1} and 703 cm^{-1} respectively.

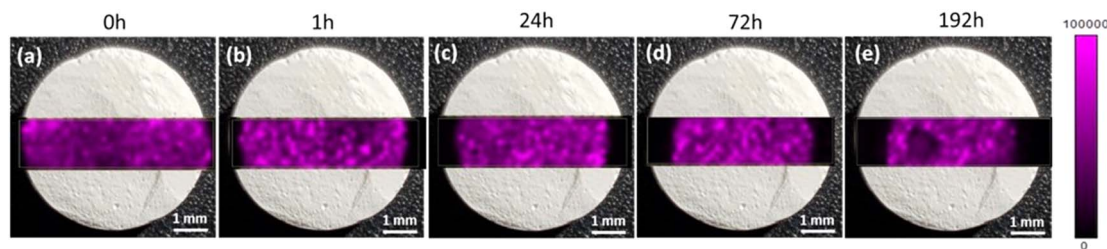


Figure 16. Distribution of GaM by Raman mapping of CPC-7G after release at 37 °C in saline solution up to 192 h (arbitrary scale).

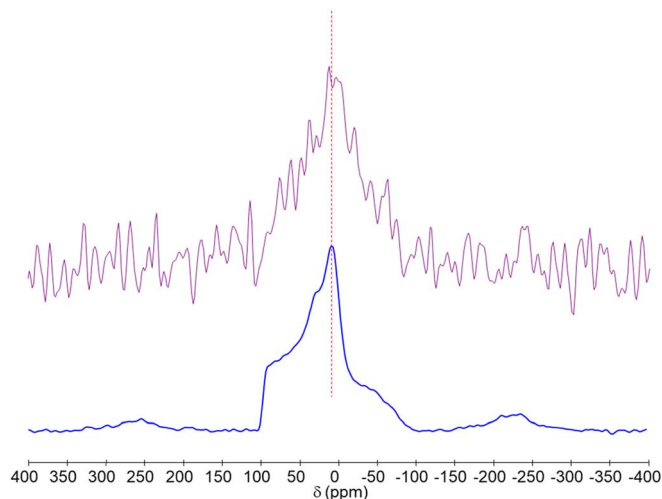


Figure 17. ^{71}Ga MAS NMR of CPC-7G after 60d. (up) versus GaM (bottom).

We observed the distribution of GaM (figure 15) as a function of the release time. For this purpose, a black-purple gradient represents the intensity of the 729 cm^{-1} band (GaM). The laser focused on the sample affected by the cutting of the cylinder (non-planar surface). For this reason, we used a lower magnification objective ($\times 20$) with a greater depth of field, and therefore, less sensitive to variations in focus. Figure 16(a) shows the homogeneous distribution of active molecules before release ($t = 0\text{ h}$). Subsequently, as it is released, the edges of the cylinders completely lose the Raman intensity of the GaM band (figures 16(b)–(e)). A strong contrast was observed between the surface that still contained GaM and that which no longer contained it. The release process occurred from the outside toward the center of the sample.

It is also possible to notice that the GaM located at the edges of the cylinder is completely dissolved by the leaching of the biomaterial by the saline solution. Notably, the representative band of Maltol, measured at 703 nm , was not observed. A ^{71}Ga MAS NMR study of a CPC-7G sample after 60 days of release and 3 days of signal acquisition showed that gallium was still present in the cement and that its chemical environment remained unchanged (figure 17).

4. Conclusion

This paper reports that gallium maltolate can be combined with up to 1.1 wt% Ga in an injectable apatitic cement. To the best of our knowledge, this is approximately four times higher than what has been described for this type of cement combined with gallium nitrate. The preparation is extremely easy because it is sufficient to add the complex directly to the powder mixture constituting the solid phase of the cement. Moreover, mixing is easier and injectability is improved owing to the intrinsic properties of the organic ligands. All characteristics of the resulting cement were almost identical to the control cement and perfectly in line with the surgeons' requirements. The gallium complex is integrated into the entire phosphocalcic matrix, and its release can be controlled over a long period. These new generations of gallium (III) compounds protected by organic ligands are extremely promising in pre-clinical studies because of their broader spectrum of use and superior

antineoplastic action compared to gallium nitrate. The combination of this type of compound with injectable bone substitutes could be useful notably for the treatment of bone tumors.

Acknowledgments

The authors would like to thank Dr J Graton (Nantes University) and Mrs F Gautier for their assistance.

Data availability statement

The data that support the findings of this study are available upon reasonable request from the authors.

Funding

Financial supports from Nantes-University (CAAPRO Project) and IR-RMN-THC FR3050 are gratefully acknowledged.

Disclosure

The authors declare that they have no competing interests.

ORCID iDs

Pascal Janvier  <https://orcid.org/0000-0001-9211-8062>

References

- [1] Soeharno H, Povegliano L and Choong P F 2018 Multimodal treatment of bone metastasis—a surgical perspective *Frontiers in Endocrinology* **9** 518
- [2] Tsuzuki S, Park S H, Eber M R, Peters C M and Shiozawa Y 2016 Skeletal complications in cancer patients with bone metastases *Int J Urol* **23** 825–32
- [3] Lopez-Heredia M A, Bernard Kamphuis G J, Thüne P C, Cumhuri Öner F, Jansen J A and Frank Walboomers X 2011 An injectable calcium phosphate cement for the local delivery of paclitaxel to bone *Biomaterials* **32** 5411–6
- [4] Guerrieri A N, Montesi M, Sprio S, Laranga R, Mercatali L, Tampieri A, Donati D M and Lucarelli E 2020 Innovative options for bone metastasis treatment: an extensive analysis on biomaterials-based strategies for orthopedic surgeons *Front. Bioeng. Biotechnol.* **8** 589964
- [5] O'Neill R, McCarthy H O, Montufar E B, Ginebra M-P, Wilson D I, Lennon A and Dunne N 2017 Critical review: injectability of calcium phosphate pastes and cements *Acta Biomater.* **50** 1–19
- [6] Tanzawa Y, Tsuchiya H, Shirai T, Nishida H, Hayashi K, Takeuchi A, Tomita K and Kawahara M 2011 Potentiation of the antitumor effect of calcium phosphate cement containing anticancer drug and caffeine on rat osteosarcoma *Journal of Orthopaedic Science* **16** 77–84
- [7] Ginebra M-P, Canal C, Espanol M, Pastorino D and Montufar E B 2012 Calcium phosphate cements as drug delivery materials *Adv. Drug Delivery Rev.* **64** 1090–110
- [8] Farbod K, Sariibrahimoglu K, Curci A, Hayrapetyan A, Hakvoort J N W, van den Beucken J J J P, Iafisco M, Margiotta N and Leeuwenburgh S C G 2016 Controlled release of chemotherapeutic platinum-bisphosphonate complexes from injectable calcium phosphate cements *Tissue Eng. Part A* **22** 788–800
- [9] Dewhurst R M, Scalzone A, Buckley J, Mattu C, Rankin K S, Gentile P and Ferreira A M 2020 Development of natural-based bone cement for a controlled doxorubicin-drug release *Front. Bioeng. Biotechnol.* **8** 754
- [10] Phull S S, Yazdi A R, Ghert M and Towler M R 2021 Bone cement as a local chemotherapeutic drug delivery carrier in orthopedic oncology: a review *Journal of Bone Oncology* **26** 100345
- [11] Harris W R and Pecoraro V L 1983 Thermodynamic binding constants for gallium transferrin *Biochemistry* **22** 292–9
- [12] Vallabhajosula S R, Harwig J F, Siemsen J K and Wolf W 1980 Radiogallium localization in tumors: blood binding and transport and the role of transferrin *J. Nucl. Med.* **21** 650–6
- [13] Warrell R P, Coonley C J, Straus D J and Young C W 1983 Treatment of patients with advanced malignant lymphoma using gallium nitrate administered as a seven-day continuous infusion *Cancer* **51** 1982–7
- [14] Warrell R P, Skelos A, Alcock N W and Bockman R S 1986 Gallium nitrate for acute treatment of cancer-related hypercalcemia: clinicopharmacological and dose response analysis *Cancer Res.* **46** 4208–12
- [15] Warrell R P, Bockman R S, Coonley C J, Isaacs M and Staszewski H 1984 Gallium nitrate inhibits calcium resorption from bone and is effective treatment for cancer-related hypercalcemia *J. Clin. Invest.* **73** 1487–90
- [16] Warrell R P, Murphy W K, Schulman P, O'Dwyer P J and Heller G 1991 A randomized double-blind study of gallium nitrate compared with etidronate for acute control of cancer-related hypercalcemia *J. Clin. Oncol.* **9** 1467–75
- [17] Cvitkovic F, Armand J-P, Tubiana-Hulin M, Rossi J-F and Warrell R P 2006 Randomized, double-blind, phase II trial of gallium nitrate compared with pamidronate for acute control of cancer-related hypercalcemia *Cancer J* **12** 47–53
- [18] Warrell R P, Israel R, Frisone M, Snyder T, Gaynor J J and Bockman R S 1988 Gallium nitrate for acute treatment of cancer-related hypercalcemia. a randomized, double-blind comparison to calcitonin *Ann. Intern. Med.* **108** 669–74

- [19] Niesvizky R 2003 Gallium nitrate in multiple myeloma: prolonged survival in a cohort of patients with advanced-stage disease *Semin Oncol* **30** 20–4
- [20] Warrell R P Jr 1997 Gallium nitrate for the treatment of bone metastases *Cancer* **80** 1680–5
- [21] Matkovic V, Apseoff G, Shepard D R and Gerber N 1990 Use of gallium to treat Paget's disease of bone: a pilot study *Lancet* **335** 72–5
- [22] Bockman R S, Wilhelm F, Siris E, Singer F, Chausmer A, Bitton R, Kotler J, Bosco B J, Eyre D R and Levenson D 1995 A multicenter trial of low dose gallium nitrate in patients with advanced Paget's disease of bone *J. Clin. Endocrinol. Metab.* **80** 595–602
- [23] Mellier C, Fayon F, Schnitzler V, Deniard P, Allix M, Quillard S, Massiot D, Boulter J M, Bujoli B and Janvier P 2011 Characterization and properties of novel gallium-doped calcium phosphate ceramics *Inorg. Chem.* **50** 8252–60
- [24] Mellier C *et al* 2015 Design and properties of novel gallium-doped injectable apatitic cements *Acta Biomater.* **24** 322–32
- [25] Strazic Geljic I, Melis N, Boukhechba F, Schaub S, Mellier C, Janvier P, Laugier J-P, Boulter J-M, Verron E and Scimeca J-C 2018 Gallium enhances reconstructive properties of a calcium phosphate bone biomaterial *J. Tissue Eng. Regen. Med.* **12** e854–66
- [26] Chitambar C R 2010 Medical applications and toxicities of gallium compounds *Int J Environ Res Public Health* **7** 2337–61
- [27] Chitambar C R 2012 Gallium-containing anticancer compounds *Future Med Chem* **4** 1257–72
- [28] Lessa J A, Parrilha G L and Beraldo H 2012 Gallium complexes as new promising metallodrug candidates *Inorg. Chim. Acta* **393** 53–63
- [29] Chitambar C R 2016 Gallium and its competing roles with iron in biological systems *Biochimica et Biophysica Acta (BBA) - Molecular Cell Research* **1863** 2044–53
- [30] Peng X-X, Gao S and Zhang J-L 2022 Gallium (III) complexes in cancer chemotherapy *Eur. J. Inorg. Chem.* **2022** 1–9
- [31] Chitambar C R, Purpi D P, Woodliff J, Yang M and Wereley J P 2007 Development of gallium compounds for treatment of lymphoma: gallium maltolate, a novel hydroxypyron gallium compound, induces apoptosis and circumvents lymphoma cell resistance to gallium nitrate *J. Pharmacol. Exp. Ther.* **322** 1228–36
- [32] Bernstein L R, Tanner T, Godfrey C and Noll B 2000 Chemistry and pharmacokinetics of gallium maltolate, a compound with high oral gallium bioavailability *Met Based Drugs* **7** 33–47
- [33] Pollina G F, Pepe M, Dean A, Marco V D and Marton D 2013 Reduction in absorption of gallium maltolate in adult horses following oral administration with food: chemistry and pharmacokinetics *Journal of Veterinary Pharmacology and Therapeutics* **36** 456–61
- [34] Fung B, Khitrin A and Ermolaev K 2000 An improved broadband decoupling sequence for liquid crystals and solids *J. Magn. Reson* **142** 97–101
- [35] Massiot D, Fayon F, Capron M, King I, Le Calvé S, Alonso B, Durand J-O, Bujoli B, Gan Z and Hoatson G 2002 Modelling one- and two-dimensional solid-state NMR spectra *Magn. Reson. Chem.* **40** 70–6
- [36] ASTM Standard C266-20, 2021 2021 *Standard Test Method for Time of Setting of Hydraulic-Cement Paste by Gillmore Needles* (West Conshohocken, PA: ASTM International) (accessed 27th, July 2022)
- [37] ASTM Standard C39M-21, 2021 2021 *Standard Test Method for Compressive Strength of Cylindrical Concrete Specimens* (West Conshohocken, PA: ASTM International) (accessed 27th, July 2022)
- [38] Mukha S A, Antipova I A, Medvedeva S, Saraev V V, Larina L I, Tsyrenzhapov A V and Sukhov B G 2007 *Synthesis and Properties of Metal Chelates Based on Natural γ -Pyrone Maltol* **15** 448–58
- [39] Allen F H 2002 The Cambridge structural database: a quarter of a million crystal structures and rising *Acta Crystallogr. B* **58** 380–8
- [40] Frisch M J *et al* 2016 *Gaussian 09, Revision D.01* (Wallingford CT: Gaussian, Inc.)
- [41] Zhao Y and Truhlar D G 2008 The M06 suite of density functionals for main group thermochemistry, thermochemical kinetics, noncovalent interactions, excited states, and transition elements: two new functionals and systematic testing of four M06-class functionals and 12 other functionals *Theor Chem Account* **120** 215–41
- [42] CCCBDB listing of precalculated vibrational scaling factors
- [43] QUALEX2.0 <https://ba.ic.cnr.it/softwareic/qualxweb> (accessed 27th, July 2022)
- [44] Legrand A P, Sfihi H, Lequeux N and Lemaitre J 2009 31P Solid-State NMR study of the chemical setting process of a dual-paste injectable *Journal of Biomedical Materials Research Part B: Applied Biomaterials* **91B** 46–54
- [45] Guo H, Pujari-Palmer M, Yu Y, Stevansson B, Engqvist H and Edén M 2020 Quantitative phase analyses of biomedical pyrophosphate-bearing monetite and brushite cements by solid-state NMR and powder XRD *Ceram. Int.* **46** 11000–12
- [46] Zhang J, Liu W, Schnitzler V, Tancret F and Boulter J-M 2014 Calcium phosphate cements for bone substitution: chemistry, handling and mechanical properties *Acta Biomater.* **10** 1035–49
- [47] Schnitzler V *et al* 2011 Investigation of alendronate-doped apatitic cements as a potential technology for the prevention of osteoporotic hip fractures: critical influence of the drug introduction mode on the *in vitro* cement properties *Acta Biomater.* **7** 759–70
- [48] Despas C, Schnitzler V, Janvier P, Fayon F, Massiot D, Boulter J-M, Bujoli B and Walcarius A 2014 High-frequency impedance measurement as a relevant tool for monitoring the apatitic cement setting reaction *Acta Biomater.* **10** 940–50
- [49] Lee K-G and Shibamoto T 2000 Antioxidant properties of aroma compounds isolated from soybeans and mung beans *J. Agric. Food Chem.* **48** 4290–3
- [50] Reffitt D M, Burden T J, Seed P T, Wood J, Thompson R P and Powell J J 2000 Assessment of iron absorption from ferric trimaltol *Ann. Clin. Biochem.* **37** 4 457–66
- [51] Kaneko N, Yasui H, Takada J, Suzuki K and Sakurai H 2004 Orally administered aluminum–maltolate complex enhances oxidative stress in the organs of mice *J. Inorg. Biochem.* **98** 2022–31
- [52] Bohner M and Baroud G 2005 Injectability of calcium phosphate pastes *Biomaterials* **26** 1553–63
- [53] Wagoner Johnson A J and Herschler B A 2011 A review of the mechanical behavior of CaP and CaP/polymer composites for applications in bone replacement and repair *Acta Biomater.* **7** 16–30
- [54] Luo J, Ajaxon I, Ginebra M P, Engqvist H and Persson C 2016 Compressive, diametral tensile and biaxial flexural strength of cutting-edge calcium phosphate cements *J. Mech. Behav. Biomed. Mater.* **60** 617–27
- [55] Brueckner T, Heilig P, Jordan M C, Paul M M, Blunk T, Meffert R H, Gbureck U and Hoelscher-Doht S 2019 Biomechanical evaluation of promising different bone substitutes in a clinically relevant test Set-Up *Materials* **12** 1364
- [56] Fuchs K F, Heilig P, McDonogh M, Boelch S, Gbureck U, Meffert R H, Hoelscher-Doht S and Jordan M C 2020 Cement-augmented screw fixation for calcaneal fracture treatment: a biomechanical study comparing two injectable bone substitutes *J Orthop Surg Res* **15** 533
- [57] Massiot D, Vosegaard T, Magneron N, Trumeau D, Montouillout V, Berthet P, Loiseau T and Bujoli B 1999 71 Ga NMR of reference GaIV, GaV, and GaVI compounds by MAS and QPASS, extension of gallium/aluminum NMR parameter correlation *Solid State Nucl. Magn. Reson.* **15** 159–69
- [58] Parker D, Waldron B P and Yufit D S 2013 Crystallographic and solution NMR structural analyses of four hexacoordinated gallium(III) complexes based on ligands derived from 6-amino-perhydro-1,4-diazepine *Dalton Trans.* **42** 8001–8

- [59] Higuchi T 1963 Mechanism of substaigned-action medication. Theoretical analysis of rate of release of solid drugs dispersed in solid matrices *J. Pharm. Sci.* **52** 1145–9
- [60] Korsmeyer R W, Gurny R, Doelker E, Buri P and Peppas N A 1983 Mechanisms of solute release from porous hydrophilic polymers *Int. J. Pharm.* **15** 25–35
- [61] Kopcha M, Tojo K J and Lordi N G 1990 Evaluation of methodology for assessing release characteristics of thermosoftening vehicles *J. Pharm. Pharmacol.* **42** 745–51
- [62] Noukrati H, Cazalbou S, Demnati I, Rey C, Barroug A and Combes C 2016 Injectability, microstructure and release properties of sodium fusidate-loaded apatitic cement as a local drug-delivery system *Mater. Sci. Eng. C: Mater. Biol. Appl.* **59** 177–84
- [63] Vidal E, Buxadera-Palomero J, Pierre C, Manero J M, Ginebra M-P, Cazalbou S, Combes C, Rupérez E and Rodríguez D 2019 Single-step pulsed electrodeposition of calcium phosphate coatings on titanium for drug delivery *Surf. Coat. Technol.* **358** 266–75